Ligand substitution effects in d^6 manganese carbonyl complexes. A comparative study of $Mn(CO)_6^+$, $Mn(CO)_5Cl$, $Mn(CO)_5^+$ and $Mn(CO)_4Cl$

K. Pierloot, P. Hoet and **L. G. Vanquickenborne***

Department of Chemistry, University of Leuven, Celestijnenlaan 200F, 3001 Heverlee (Belgium)

(Received November 15, 1990)

Abstract

Hartree–Fock Roothaan calculations are reported for the ground state and the ligand field excited states of the hexacoordinated complexes $Mn(CO)_6^+$ and $Mn(CO)_5Cl$, and the pentacoordinated square pyramids $Mn(CO)_5^+$ and $Mn(CO)_4Cl$. The results are used to discuss the validity of the ligand field approach in these organometallics, and the two lowest-lying features in the UV–Vis spectrum of $Mn(CO)_5Cl$ have been assigned as ligand field $^1A_1 \rightarrow {}^1E$ transitions.

I. Introduction

When dealing with transition metal chemistry a clear distinction is often made between classical Werner type complexes and complexes of π-acid ligands [1, 2]. The distinction between both types of species is mainly connected to the formal oxidation number of the central metal ion. Classical complexes are characterized by high oxidation numbers (+2, +3 or even higher), whereas complexes with π-acid ligands tend to have metal atoms with low (+1, 0 and even negative) formal oxidation numbers.

The bonding in classical Werner type complexes can be described rather adequately by ligand field theory. Due to the high oxidation number of the metal ion, the valence 3d shell is energetically well separated from the 4s and 4p orbitals; also, the actual overlap between the metal 3d orbitals and the ligand σ and π orbitals is very limited in these complexes. Both facts justify the use of a model in which the ligand field is considered as a perturbation potential on the valence 3d orbitals. Furthermore, if one assumes the perturbation potential to be additive in the individual ligand contributions, only a limited set of parameters is needed for the description of related complexes, which makes the method very attractive. In a number of previous studies on hexacoordinated complexes of Cr(III) and Co(III), containing simple ligands such as F^-, OH^- and CN^-, it was shown that the basic postulates of ligand field theory are to a large extent substantiated from an *ab initio* point of view [3, 6].

In complexes containing π-acid ligands however, the situation is more complicated; π-acid or π-acceptor ligands are characterized by low-lying vacant π orbitals, being able to accept electron density from filled metal orbitals, and thereby delocalizing the large electron density on the metal atom (necessarily in low oxidation states) onto the ligands. This π-charge transfer induces an M^+–L^- polarity that is counterbalanced by an enhanced σ electron donation from the ligand. Both bonding and 'backbonding' involve significant overlap of the metal d-orbitals with the ligands, in contrast with the bonding type proposed for the classical Werner complexes. Also, due to the low valency of the central metal ion, the 3d–4s and 3d–4p energy separations are much smaller in π-acceptor complexes [7]. Therefore, rather than by the application of ligand field theory, the bonding in the complexes under consideration is very often described qualitatively by using the alternative valence bond model, with nd–(n+1)s–(n+1)p hybrid orbitals on the central metal ion, and by using the 18-electron rule as a guiding principle [1].

However, some aspects of the chemistry and especially of the photochemistry of π-acid complexes can still better be described when starting from a ligand field picture. The lowest excited states in most

*Author to whom correspondence should be addressed.

0020-1693/91/$3.50

π-acceptor complexes correspond to 'ligand field type' transitions, and the corresponding states serve as the precursors of photochemical substitution reactions. A number of π-acceptor ligands have been included with some success into the ligand field method by allowing negative π parameters [1, 8].

It is the purpose of the present work to examine from an *ab initio* point of view as to how far the concepts of ligand field theory remain valid in complexes containing π-acceptor ligands. More specifically, we will present the results of a comparative analysis of $Mn(CO)_6^+$ with the three complexes $Mn(CO)_5Cl$, $Mn(CO)_5^+$ and $Mn(CO)_4Cl$. The latter two complexes are pentacoordinated square pyramids; they are the results of a CO dissociation from $Mn(CO)_6^+$ and from the position *trans* to Cl in $Mn(CO)_5Cl$, respectively. It has by no means been our intention to present results which are in quantitative agreement with experiment: all calculations have been performed at the Hartree–Fock level, and no geometry optimizations on the different hexa- and pentacoordinated species have been performed. Instead we want to focus on the effects of ligand substitution in, and ligand removal from the octahedral $Mn(CO)_6^+$ complex, both with respect to the ground state electronic structure and the ligand field spectrum. The validity of the two basic postulates of ligand field theory (ligand additivity and the nearly pure 3d-character of the valence shell orbitals) will be critically examined.

II. Calculational details

The SCF calculations were carried out within the framework of Roothaan's RHF openshell formalism [9], using the SYMOL program [10]. Although an accurate calculation would require a complete geometry optimization for each structure, we decided to perform all calculations on somewhat idealized geometries, keeping all ligand–metal–ligand bond axes at 90°, and using only one set of bond distances, namely 2.369 Å for Mn–Cl, 1.841 Å for Mn–C and 1.124 Å for C–O. These are the average bond lengths for the $Mn(CO)_5Cl$ complex that resulted from a number of experimental measurements [11–13].

For $Mn(CO)_6^+$ itself, experimental bond lengths are not available. Normally however one would expect the Mn–C distance to be slightly longer than the distances in $Mn(CO)_5Cl$ and closer to the Cr–C value of 1.91 Å in $Cr(CO)_6$. Indeed, it has been observed that in Group VI and VIIB metal carbonyl complexes ligands with less π-accepting capabilities than CO tend to strengthen the $Mn–C_{trans}$ and, to a lesser extent, also the $Mn–C_{cis}$ bond [14]. In fact, the experimental $Mn–C_{trans}$ bond in $Mn(CO)_5Cl$ is about 0.08 Å shorter than the $Mn–C_{cis}$ bond (the $C_{trans}–Mn–C_{cis}$ bond angle is 92°) [13]. We have to realize of course that by averaging the Mn–C distance over CO_{cis} and CO_{trans} we will necessarily lose some information regarding the directional character of the ground state effect caused by replacing CO by Cl^- in $Mn(CO)_6^+$.

The geometry of the pentacoordinated species was taken to be a flat square pyramid, with Cl^- in the apical position of $Mn(CO)_4Cl$, thereby allowing no geometrical relaxation whatsoever after the dissociation of CO from the hexacoordinated complexes $Mn(CO)_6^+$ and $Mn(CO)_5Cl$. No structural experimental data are available for $Mn(CO)_5^+$, but for the related species $Cr(CO)_5$ [15a] and $Mn(CO)_5$ [15b] IR spectroscopic measurements in frozen gas matrices have indicated a C_{4v} square pyramid structure with an axial–equatorial bond angle only slightly greater than 90° (92°–96°). As for $Mn(CO)_4Cl$, it was shown [15c, 16] that the actual structure should be closer to a trigonal bipyramid (C_{2v} symmetry) with Cl^- in equatorial position. Yet, as the focus of the present paper is on the application of ligand field ideas (such as ligand additivity), we will postpone a study of trigonal bipyramids until later [17].

The first-row atoms C and O were described by the Huzinaga–Dunning basis set (9s 5p/5s 3p) [18]. For the Cl atom, we used the (12s 9p/6s 5p) non-segmented basis set, introduced by Dunning [19]. For the Mn atom, we decided to use a (15s 11p 6d/9s 6p 4d) non-segmented basis set. This set was obtained starting from the (15s 11p 6d/10s 8p 4d) segmented basis set described elsewhere [20], by duplicating the second s-type and the second and fifth p-type CGTF, respectively, and grouping these functions with both the preceding and the following contracted function. The procedure we used in determining the contribution of the shared basis function in each one of the contracted functions is slightly different from the method used by Dunning [19] and is described in the Appendix, where also the resulting contraction coefficients are given in a separate Table. By using this procedure we reduced the number of contracted functions considerably without any significant loss in precision. Thus we calculated the total energy of the $Mn(CO)_6^+$ complex using both the new (15s 11p 6d/9s 6p 4d) and the original (15s 11p 6d/10s 8p 4d) basis sets. The resulting energies are -1825.6080 Ha and -1825.6085 Ha, respectively.

In Table 1, some information is given regarding the symmetry properties of the calculated structures. For each structure, an SCF calculation was performed

TABLE 1. Symmetry properties and notation of the octahedral complex $Mn(CO)_6^+$ and the C_{4v} complexes $Mn(CO)_5Cl$, $Mn(CO)_5^+$ and $Mn(CO)_4Cl$ (for further reference in the other Tables)

Reduction of the octahedral irreducible representations O_h	→	C_{4v}
a_{1g}	→	a_1
e_g	→	a_1+b_1
t_{1g}	→	a_2+e
t_{2g}	→	b_2+e
t_{1u}	→	a_1+e
t_{2u}	→	b_1+e

Basis functions of the irreducible representations[a] O_h	Mn orbitals	CO orbitals
a_{1g}	s	σ
e_g	d_{z^2}, $d_{x^2-y^2}$	σ
t_{1g}		π
t_{2g}	d_{xz}, d_{yz}, d_{xy}	π
t_{1u}	p_x, p_y, p_z	σ; π
t_{2u}		π

C_{4v}	Mn orbitals	CO_{eq}	CO_{ax}	Cl
a_1	s; p_z; d_{z^2}	σ; $\pi_\perp$	σ	s; p_σ
a_2		$\pi_\parallel$		
b_1	$d_{x^2-y^2}$	σ; $\pi_\perp$		
b_2	d_{xy}	$\pi_\parallel$		
e	p_x, p_y; d_{xz}, d_{yz}	σ; $\pi_\perp$; $\pi_\parallel$	π	p_π

[a]In the C_{4v} complexes, the z axis is the fourfold axis, containing the Cl^- ligand in the case of $Mn(CO)_5Cl$ and $Mn(CO)_4Cl$. The subscript ax refers to the axial CO ligand (on the z axis) in $Mn(CO)_5Cl$ and $Mn(CO)_5^+$; the subscript eq refers to the equatorial ligands (in the xy plane). The notation $\pi_\perp$ and $\pi_\parallel$ designates CO π orbitals having their nodal plane perpendicular or parallel to the z axis.

on all states corresponding to the octahedral t_{2g}^6 and $t_{2g}^5e_g^1$ configurations. $Mn(CO)_6^+$ itself is characterized by a $^1A_{1g}(t_{2g}^6)$ closed-shell ground state, while the first excited configuration $t_{2g}^5e_g^1$ gives rise to two singlet state $^1T_{1g}$ and $^1T_{2g}$, and two triplet states $^3T_{1g}$ and $^3T_{2g}$. As can be seen from Table 1, these states are further split by the $O_h \rightarrow C_{4v}$ symmetry reduction: the T_{1g} states into $E+A_2$, the T_{2g} states into $E+B_2$.

III. Results and discussion

A. Characteristics of the $^1A_1$ states

The total energy of the closed-shell $^1A_1$ states of the different complexes is given in Table 2. Hereby it should be noted that this $^1A_1$ state is not found

TABLE 2. Total energy E and orbital energy of the topmost (fully occupied) orbitals of the four complexes under consideration, in their $^1A_1$ states[a]

$Mn(CO)_6^+(^1A_{1g})$ $E=-1825.6080$		$Mn(CO)_5^+(^1A_1)$ $E=-1712.8955$		$Mn(CO)_5Cl(^1A_1)$ $E=-2172.6831$		$Mn(CO)_4Cl(^1A_1)$ $E=-2059.9704$	
Symmetry	Energy	Symmetry	Energy	Symmetry	Energy	Symmetry	Energy
				13e[π(Cl)]	−0.3785	12e[π(Cl)]	−0.3756
				21a_1[σ(Cl)]	−0.4168	16a_1[σ(Cl)]	−0.4115
$2t_{2g}$[3d(Mn)]	−0.6339	2b_2[3d_{xy}(Mn)]	−0.6182	2b_2[3d_{xy}(Mn)]	−0.4392	2b_2[3d_{xy}(Mn)]	−0.4101
		11e[3d_{xz},3d_{yz}(Mn)]	−0.6441	12e[3d_{xz},3d_{yz}(Mn)]	−0.4740	11e[3d_{xz},3d_{yz}(Mn)]	−0.4811
$8t_{1u}$[σ(CO), π(CO)]	−0.7980	10e[σ(CO)$_{eq}$; $\pi_\parallel$(CO$_{eq}$]	−0.8023	11e[σ(CO)$_{eq}$; $\pi_\parallel$(CO$_{eq}$]	−0.6418	10e[σ(CO); $\pi_\parallel$(CO)]	−0.6402
		16a_1[σ(CO)$_{ax}$; $\pi_\perp$(CO$_{eq}$]	−0.8112	20a_1[σ(CO)$_{ax}$; $\pi_\perp$(CO$_{eq}$]	−0.6583	15a_1[$\pi_\perp$(CO)]	−0.6859
$1t_{1g}$[π(CO)]	−0.8315	1a_2[$\pi_\parallel$(CO)$_{eq}$]	−0.8327	6b_1[σ(CO)$_{eq}$]	−0.6605	6b_1[σ(CO)]	−0.6552
		9e[π(CO)$_{ax}$; $\pi_\perp$(CO$_{eq}$]	−0.8357	1a_2[$\pi_\parallel$(CO$_{eq}$]	−0.6768	1a_2[$\pi_\parallel$(CO)]	−0.6744
$5e_g$[σ(CO)]	−0.8317	6b_1[σ(CO$_{eq}$]	−0.8303	5b_1[$\pi_\perp$(CO$_{eq}$]	−0.6852	5b_1[$\pi_\perp$(CO)]	−0.6790
$1t_{2u}$[π(CO)]	−0.8419	5b_1[$\pi_\perp$(CO)$_{eq}$]	−0.8395	10e[π(CO)$_{ax}$; $\pi_\perp$(CO)$_{eq}$]	−0.6868	9e[$\pi_\perp$(CO)]	−0.6899
		8e[π(CO)$_{eq}$]	−0.8589	9e[π(CO)$_{eq}$]	−0.7006	8e[σ(CO); $\pi_\parallel$(CO)]	−0.7019
$7t_{1u}$[σ(CO), π(CO)]	−0.8761	15a_1[σ(CO)$_{ax}$; $\pi_\perp$(CO$_{eq}$]	−0.8630	19a_1[σ(CO)$_{ax}$; $\pi_\perp$(CO$_{eq}$]	−0.7019		
		7e[π(CO)$_{ax}$; σ(CO)$_{eq}$; π(CO$_{eq}$]	−0.8767	1b_2[$\pi_\parallel$(CO$_{eq}$]	−0.7179	1b_2[$\pi_\parallel$(CO)]	−0.7144
$1t_{2g}$[π(CO)]	−0.8769	1b_2[$\pi_\parallel$(CO$_{eq}$]	−0.8768	8e[π(CO)$_{ax}$; σ(CO)$_{eq}$; π(CO)$_{eq}$]	−0.7292		
$8a_{1g}$[σ(CO)]	−0.9281	14a_1[σ(CO)$_{ax}$; σ(CO)$_{eq}$]	−0.9221	18a_1[σ(CO)$_{ax}$; σ(CO)$_{eq}$]	−0.7672	14a_1[σ(CO)]	−0.7468

[a]All energies are in hartrees. The dominant character of the orbitals is shown in brackets. The position of the ligands and the different subscript notations are as denoted in Table 1.

to be the ground state in every case: for $Mn(CO)_4Cl$ the ^3E state, corresponding to the $3d_{xz,yz} \rightarrow 3d_{z^2}$ transition was calculated slightly below the $^1A_1$ state. This point will be further examined in the following sections, where the excited states are discussed. In the present section we will confine ourselves to a comparison of the different complexes in their $^1A_1(t_{2g}^6)$ states.

Table 2 also shows the energy and the dominant atomic orbital character of the valence MOs. In $Mn(CO)_6^+$ and $Mn(CO)_5^+$ the highest filled molecular orbitals are metal 3d-type orbitals. In the monochloro–pentacarbonyl complex, it can be seen that two molecular orbitals of predominant chlorine character show up above these metal-type orbitals, while in the monochloro–tetracarbonyl complex both types of orbitals are mixed. The sequence of the orbitals in $Mn(CO)_5Cl$ is quite similar as calculated by Guest *et al.* [14], using a much smaller basis set. The actual orbital energies differ by at most 0.05 Ha.

The most striking point of Table 2 is the large energy shift of all orbitals, accompanying the replacement of one CO ligand by Cl^-, both in $Mn(CO)_6^+$ and $Mn(CO)_5^+$. Apart from some slight rearrangements, this substitution seems to shift all molecular orbitals uniformly upward by 0.16 to 0.18 Ha. This shift must be attributed to a charge effect, caused by substituting the neutral CO by a negatively charged Cl^- ligand. A similar energy shift could probably be obtained by the introduction of a negative counterion in the charged complexes $Mn(CO)_6^+$ and $Mn(CO)_5^+$ [21, 22]. No analogous large energy shift occurs when one CO ligand is simply removed from $Mn(CO)_6^+$, without replacing it by another ligand: the general features of the orbitals are essentially the same in $Mn(CO)_5^+$ as they are in the parent octahedral compound $Mn(CO)_6^+$. The low-lying orbitals are essentially unshifted, while for the high-lying valence orbitals the energy shifts amount to no more than a few hundreths of a Hartree. A comparison of both neutral complexes $Mn(CO)_5Cl$ and $Mn(CO)_4Cl$ reveals a similar situation.

TABLE 3. Calculated and experimental ionization energies (in eV) of the topmost four orbitals of $Mn(CO)_5Cl$

Orbital	Calculated orbital energy	Experimental [23]
13e[π(Cl)]	10.30	8.94
21a_1[σ(Cl)]	11.34	9.56
2b_2[$3d_{xy}$(Mn)]	11.95	11.18
12e[$3d_{xz}$,$3d_{yz}$(Mn)]	12.90	10.56

TABLE 4. Orbital populations and charges q on the central Mn atom and on the different ligands in the $^1A_1$ states of the four complexes under consideration

	$Mn(CO)_6^+$	$Mn(CO)_5^+$	$Mn(CO)_5Cl$	$Mn(CO)_4Cl$
Mn				
$3d_{z^2}$	0.65	0.33	0.58	0.27
$3d_{x^2-y^2}$	0.65	0.58	0.56	0.49
$3d_{xy,yz}$	3.55	3.68	3.67	3.88
$3d_{xy}$	1.77	1.75	1.71	1.66
4s	0.00	0.07	0.23	0.19
$4p_z$	−0.04	0.04	0.00	0.18
$4p_{x,y}$	−0.08	0.08	0.17	0.20
q_{Mn}	0.52	0.51	0.11	0.19
CO_{eq}				
σ	9.72	9.74	9.73	9.76
π	4.20	4.18	4.20	4.18
$q_{CO_{eq}}$	0.08	0.10	0.07	0.06
CO_{ax}				
σ	9.72	9.72	9.75	
π	4.20	4.19	4.24	
$q_{CO_{ax}}$	0.08	0.10	0.01	
Cl				
s, p_σ			9.56	9.59
p_π			7.85	7.85
q_{Cl}			−0.40	−0.42

In Table 3, the calculated orbital energies of the topmost four orbitals of $Mn(CO)_5Cl$ are compared to the corresponding ionization potentials in the experimental photoelectron spectrum of this complex [23]. As was already noticed in ref. 14, the calculated energy sequence does not fully agree with the relative ordering of the experimental ionization potentials. The calculations do agree with experiment in assigning the first two bands to ionizations from orbitals with mainly halogen character, and the next two bands to ionizations from the 3d-type orbitals. Yet, for the latter, calculations suggest that the 12e orbital is more tightly bound than the $2b_2$ orbital, while the assignment of the spectrum on intensity arguments yields a reversal of this order. Apparently, a greater relaxation is associated with ionization from the metal e than from the b_2 orbital. It is noteworthy that the calculated order of the 3d-type orbitals in $Mn(CO)_5Cl$ and in the five-coordinated complexes also seems to be in disagreement with ligand field arguments. Indeed, assuming that CO has a negative π-parameter, ligand field theory predicts an energy ordering $b_2 < e$ in the three C_{4v} complexes. Hartree–Fock calculations are known to yield the wrong orbital level order (as compared to ligand field expressions)

in other substituted complexes as well [6]. As was the case there, the situation will be reversed at the state level.

The populations in the central metal valence orbitals and in the ligand σ and π orbitals for the four complexes under consideration are shown in Table 4. Due to the fact that our calculations were performed with rather large basis sets, the results of Table 4 must certainly be interpreted with some care. Yet, apart from the fact that it offers a means for comparison with earlier work, a number of important general observations regarding the bonding in the different complexes can be made from this Table.

(1) The net charge of the different carbonyl ligands is slightly positive in all cases, ranging from 0.01 to 0.10. Our results thus indicate that more electronic charge is shifted to the central Mn atom through the σ bond than in the opposite direction through the π bond. In $Mn(CO)_6^+$ this charge transfer seems to take place exclusively in the metal 3d orbitals, while in the other complexes some participation of the 4s and 4p orbitals is apparent. As we shall see in Section IIIC, the participation of these orbitals in the bonding will turn out to be much more important for those excited states that result from a $3d\pi \rightarrow a_1$ ($\sim 3d_{z^2}$) excitation.

The result for CO in Table 4 is only slightly different from the one given by Guest *et al.* [14] for $Mn(CO)_5Cl$ and other monosubstituted $Mn(CO)_5L$ complexes (with $L = H^-$, CH_3^- and CN^-). In each one of these complexes Guest *et al.* calculated CO with a slightly negative charge of about -0.10 to -0.18 e. The difference with our result is mainly due to the fact that their use of a small basis set leads to a description of CO as a weaker σ donor: in $Mn(CO)_5Cl$ for example they found only 0.1 e^- to be transferred from the CO σ orbitals to the central Mn atom.

Fenske–Hall type calculations [24] on $Mn(CO)_6^+$ and $Mn(CO)_5Cl$ on the other hand do lead to results that are quite different from ours, characterizing CO both as a much stronger σ donor and a much stronger π acceptor. More remarkable however is the fact that the Fenske–Hall calculations result in very large 4p populations on the central Mn atom (1.383 e^- in $Mn(CO)_6^+$, 1.282 e^- in $Mn(CO)_5Cl$). This result is obviously not confirmed by large-basis Hartree–Fock calculations.

(2) In contrast to both the results from Guest *et al.* [14] and Fenske and De Kock [24], we do calculate Cl^- as a π donor. From the results of Table 4 one can see that both in $Mn(CO)_5Cl$ and $Mn(CO)_4Cl$, the Cl^- ligand is left with a p_π population of only 7.85 electrons. In ref. 24 this population is exactly 8 electrons, while in ref. 14 Cl^- is even calculated as a weak π acceptor, with a p_π population of 8.04 electrons. Our result is certainly more in line with the conventional interpretation of ligand field spectral data, characterizing Cl^- as a π donor both in Co(III) and Cr(III) complexes [25]. The results of Table 4 for the Cl σ orbitals suggest that Cl^- should be classified as a stronger σ donor than CO, since 0.41 to 0.44 electrons are transferred from the Cl σ orbitals to the central metal ion, whereas CO is seen to donate only 0.24 to 0.28 electrons through its σ bond. However, the charge shift phenomena are certainly strongly influenced by the fact that Cl^- has a net negative charge (as opposed to CO). Moreover, since the σ and π characteristics of a ligand are usually inferred from spectral data, this point will be resumed in the next section, where the excited ligand field states in the different complexes will be analyzed.

(3) According to the population results the classical idea of ligand additivity seems to hold to a large extent also for the π-acid complexes under consideration. Indeed, the σ and π populations of the CO_{eq}, CO_{ax} and Cl^- ligands show very little variation on the removal of one CO ligand from $Mn(CO)_6^+$ or $Mn(CO)_5Cl$. This is a rather surprising result, since it runs counter to the usual π-backbonding argument, which states that the extent of π-backbonding to a CO group should increase as the π-acceptor ability of a heteroligand competing for backbonding electrons decreases. Following this argument, one would expect that the dissociation of one CO group would lead to a significantly increased backbonding to the *trans* carbonyl group, and to a lesser extent also to the *cis* carbonyl groups. Table 3 shows that this expectation turns out to be wrong, and that instead, ligand additivity prevails. Yet, the above idea of mutual interactions between ligands with different π-acceptor characteristics does seem to have some validity in $Mn(CO)_5Cl$. As one can see from the results in Table 4, the substitution of CO by a π-donor in $Mn(CO)_6^+$ makes a small contribution to the π population of its *trans* counterpart, though it does not affect the π population of the *cis* CO groups. This result should of course be seen in its proper perspective, and considering that all calculations were performed with equal Mn–CO distances. Yet, the results in Table 4 suggest a relative strengthening of the $Mn–CO_{trans}$ bond in $Mn(CO)_5Cl$ relative to the $Mn–CO_{cis}$ bonds. In a recent Hartree–Fock study on the substitution effect of Cl on the dissociation rate of CO in $Mn(CO)_5Cl$ it was shown that ground state effects do indeed slightly favour a *cis* CO dissociation [16]. Starting from an optimized ground state geometry, and al-

lowing no relaxation during the dissociation, the difference between the activation energy for *trans*- and *cis*-CO loss amounts to 2.3 kcal/mol. Yet, it was shown [16] that the largest part of the *cis*-CO labilization in $Mn(CO)_5Cl$ is caused by relaxation effects.

(4) The central metal atomic orbital populations do show some variation between the different complexes. A striking point for example is the fact that the population of the $3d_{z^2}$ orbital is decreased to about half its original value when one axial CO ligand is removed, both from $Mn(CO)_6^+$ and $Mn(CO)_5Cl$. The population in the $3d_{xz,yz}$ shell qualitatively follows the corresponding trend: due to the absence of one π accepting CO the population in these orbitals is slightly raised, with 0.12 to 0.20 electron. The presence of the axial ligands also seems to affect the 3d populations in the equatorial plane, though the effect is less pronounced: the $3d_{x^2-y^2}$ population and, to a lesser extent also the $3d_{xy}$ population, is lower in the C_{4v} complexes than in $Mn(CO)_6^+$. However, this decrease is largely compensated by the simultaneous increase in the 4s and 4p populations, leaving the equatorial CO ligands unaffected.

In conclusion, one can say that the Hartree–Fock results for the $^1A_1$ state in the complexes under consideration are reasonably well in line with an additive, d-only ligand field picture. The absence of ligand substitution effects on the bonding properties of the inert ligands is confirmed; the 4s and 4p orbitals, do not seem to affect the metal–ligand bonding to a great deal either. In the next sections however, we will show that the mixing of the 4s and 4p orbitals in the 3d shell does have a very pronounced effect on the ligand field spectrum of the C_{4v} complexes, and even leads to the prediction of a ^3E ground state in $Mn(CO)_4Cl$.

B. Description of the excited ligand field states

The experimental data on the ligand field transitions in both $Mn(CO)_6^+$ and $Mn(CO)_5Cl$ are limited, due to the appearance in their electronic spectra of very intense charge transfer bands [26, 27]. In a previous paper [28] we have identified the band at 39 600 cm^{-1} in the experimental spectrum of $Mn(CO)_6^+$ as the transition $^1A_{1g} \rightarrow {}^1T_{2g}$. The electronic absorption spectrum of $Mn(CO)_5Cl$ shows two weak bands, at 26 520 and 37 000 cm^{-1}, respectively (in CH_3OH solution) [27]. Based on the interpretation of the photoelectron spectrum of $Mn(CO)_5Cl$, these bands were originally ascribed to transitions from the highest occupied 13e[π(Cl)] orbital to antibonding carbonyl π-orbitals [27]. Yet, in more recent literature [29], it is generally accepted that the lowest transitions in $Mn(CO)_5Cl$ and other monosubstituted manganese carbonyl complexes correspond to ligand field transitions.

Table 5 and Fig. 1 show the calculated transition energy of the lowest excited states in the four complexes under consideration, corresponding to the $t_{2g}^5 e_g^1$ configuration of octahedral parentage. Table 5 also includes the first-order ligand field expressions corresponding to the different transitions.

In an additive ligand field model the three C_{4v} complexes $Mn(CO)_5Cl$, $Mn(CO)_5^+$ and $Mn(CO)_4Cl$ can be described with only one set of ligand field expressions. These expressions are given in terms of

TABLE 5. Hartree–Fock transition energies (in cm^{-1}) of the ligand field states corresponding to the octahedral $t_{2g}^5 e_g^1$ configuration, for the hexacoordinated complexes $Mn(CO)_6^+$ and $Mn(CO)_5Cl$ and the pentacoordinated complexes $Mn(CO)_5^+$ and $Mn(CO)_4Cl$. For each excited state, the corresponding orbital transition is explicitly specified[a]

State	First-order LFT O_h	SCF $Mn(CO)_6^+$	State	First-order LFT C_{4v}	SCF		
					$Mn(CO)_5Cl$	$Mn(CO)_5^+$	$Mn(CO)_4Cl$
$^1A_{1g}$	0	0	$^1A_1$	0	0	0	0
$^3T_{1g}(pq \rightarrow p^2{-}q^2)$	$10Dq - 3C$	27488	$^3E_a(xz,yz \rightarrow z^2)$	$10Dq - \Delta\sigma + \Delta\pi - 3C + 2B$	18478	7615	−514
			$^3A_2(xy \rightarrow x^2{-}y^2)$	$10Dq - 3C$	27620	27760	29315
$^1T_{1g}(pq \rightarrow p^2{-}q^2)$	$10Dq - C$	32787	$^1E_a(xz,yz \rightarrow z^2)$	$10Dq - \Delta\sigma + \Delta\pi - C + 4B$	26230	15702	8041
			$^1A_2(xy \rightarrow x^2{-}y^2)$	$10Dq - C$	32657	33042	33377
$^3T_{2g}(pq \rightarrow r^2)$	$10Dq - 3C + 8B$	33905	$^3B_2(xy \rightarrow z^2)$	$10Dq - \Delta\sigma - 3C + 8B$	26208	12497	11994
			$^3E_b(xz,yz \rightarrow x^2{-}y^2)$	$10Dq + \Delta\pi - 3C + 6B$	24811	27988	21640
$^1T_{2g}(pq \rightarrow r^2)$	$10Dq - C + 16B$	44372	$^1B_2(xy \rightarrow z^2)$	$10Dq - \Delta\sigma - C + 16B$	37782	18450	14636
			$^1E_b(xz,yz \rightarrow x^2{-}y^2)$	$10Dq + \Delta\pi - C + 12B$	35642	39014	33537

[a]For the octahedral complex, p, q and r each stand for x, y and z. The $O_h \rightarrow C_{4v}$ symmetry reduction results in two close-lying E states (E_a and E_b; both singlet and triplet). Configuration interaction between these states will result in wave functions that more closely resemble the octahedral $T_{1g}(pq \rightarrow p^2{-}q^2)$ and $T_{2g}(pq \rightarrow r^2)$ wave functions.

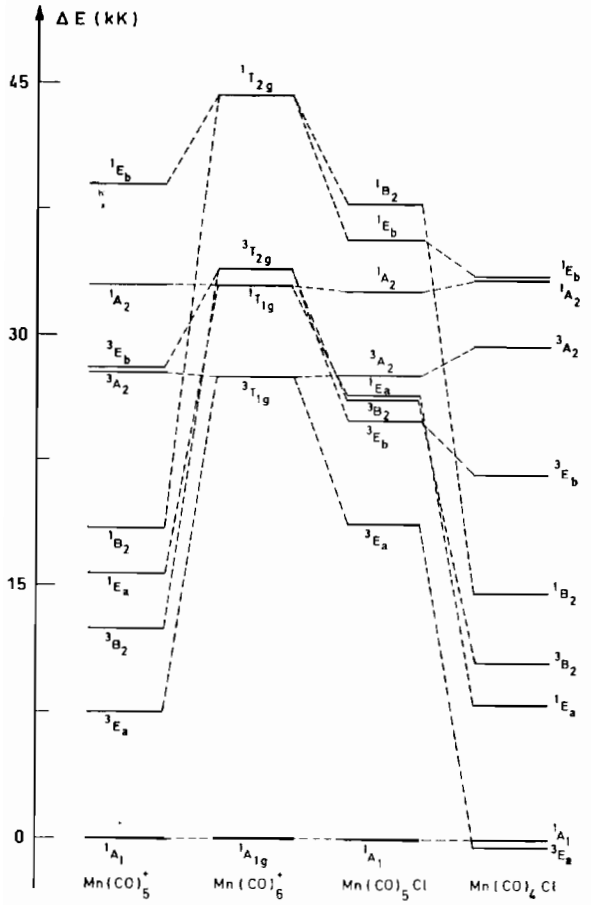

Fig. 1. State correlation diagram of the Hartree–Fock levels for the four complexes under consideration, belonging to the octahedral t_{2g}^6 and $t_{2g}^5e_g^1$ configurations. the four $^1A_{1g}$ states were arbitrarily set an equal energy.

three ligand field parameters $10Dq$, $\Delta\sigma$ and $\Delta\pi$, and the two Racah parameters B and C. Here, $10Dq$ represents the ligand field strength of CO, while $\Delta\sigma$ and $\Delta\pi$ are given by the following general expression:

$$\Delta\sigma = 2(\bar{\sigma}_{eq} - \bar{\sigma}_{ax})$$
$$\Delta\pi = 2(\bar{\pi}_{eq} - \bar{\pi}_{ax}) \quad (1)$$

where $\bar{\sigma}_{ax}$ and $\bar{\pi}_{ax}$ describe the average effect of the $+z$ and $+z$ ligand in the C_{4v} complexes, while $\bar{\sigma}_{eq}$ and $\bar{\pi}_{eq}$ contain the average effect of the four ligands in the equatorial plane. The complexes under consideration all have the same equatorial plane, containing four CO ligands. Therefore

$$\bar{\sigma}_{eq} = \sigma_{CO}$$
$$\bar{\pi}_{eq} = \pi_{CO} \quad (2a)$$

They have different axial properties however:

$Mn(CO)_6^+$: $\bar{\sigma}_{ax} = \sigma_{CO}$	$\bar{\pi}_{ax} = \pi_{CO}$
$Mn(CO)_5^+$: $\bar{\sigma}_{ax} = (\frac{1}{2})\sigma_{CO}$	$\bar{\pi}_{ax} = (\frac{1}{2})\pi_{CO}$
$Mn(CO)_5Cl$: $\bar{\sigma}_{ax} = (\frac{1}{2})(\sigma_{CO} + \sigma_{Cl})$	$\bar{\pi}_{ax} = (\frac{1}{2})(\pi_{CO} + \pi_{Cl})$
$Mn(CO)_4Cl$: $\bar{\sigma}_{ax} = (\frac{1}{2})\sigma_{Cl}$	$\bar{\pi}_{ax} = (\frac{1}{2})\pi_{Cl}$

(2b)

Using these equations, we can rewrite $\Delta\sigma$ and $\Delta\pi$ for the three C_{4v} complexes, as follows:

$Mn(CO)_5^+$: $\Delta\sigma = \sigma_{CO}$	$\Delta\pi = \pi_{CO}$
$Mn(CO)_5Cl$: $\Delta\sigma = \sigma_{CO} - \sigma_{Cl}$	$\Delta\pi = \pi_{CO} - \pi_{Cl}$
$Mn(CO)_4Cl$: $\Delta\sigma = 2\sigma_{CO} - \sigma_{Cl}$	$\Delta\pi = 2\pi_{CO} - \pi_{Cl}$

(3)

We now return to the state correlation diagram in Fig. 1 and the corresponding ligand field expressions in Table 5. Some of the general features of the Hartree–Fock levels indeed conform with the predictions of ligand field theory.

(1) The position of the $A_2(xy \rightarrow x^2-y^2)$ levels (both $^1A_2$ and $^3A_2$) remains practically constant throughout the series of four complexes. This means that also at the Hartree–Fock level the spectrochemical strength in the equatorial plane is essentially independent of the presence of axial ligands. This fact has been noticed before in the study of the substitution of CN^- by OH^- in hexacoordinated Co(III) cyanide complexes [5, 6]. Now we can extend this conclusion even further, since apparently at the Hartree–Fock level even the complete removal of one axial ligand does not affect the equatorial spectrochemical strength to any significant extent. This conclusion is in line with the absence of any ground state *cis*-effect, discussed in the previous section.

(2) Some information regarding the *ab initio* value of the π parameters can be obtained from the energy evolution of the $E_b(xz,yz \rightarrow x^2-y^2)$ states (again both ^3E_b and ^1E_b) between the different complexes. Thus from Fig. 1 one can see the following energy sequence for these states in the C_{4v} complexes:

$$E_b\text{: } E[Mn(CO)_5^+] > E[Mn(CO)_5Cl] > E[Mn(CO)_4Cl] \quad (5)$$

This energy sequence can only be rationalized by a positive π_{Cl} value (of about 3300 cm^{-1}) and a negative value for π_{CO} (with a mean value of about -2600 cm^{-1}). As a matter of fact, these numerical π values describe the energy change of the E_b states accompanying the dissociation of Cl^- or CO from $Mn(CO)_5Cl$, leading to $Mn(CO)_5^+$ and $Mn(CO)_4Cl$, respectively. The Hartree–Fock state calculations thus at least qualitatively confirm the ligand field concept of assigning a negative π-parameter to π-acid ligands.

(3) In all three C_{4v} species the equatorial σ-donation is significantly larger than the axial σ-donation ($\Delta\sigma > 0$). This can be deduced from the relative position of both $^{1,3}E$ states: $^{1,3}E_a$ always correspond to a ($xz,yz \rightarrow z^2$) transition, $^{1,3}E_b$ to a ($xz,yz \rightarrow x^2-y^2$) transition. (Configuration interaction between $^{1,3}E_a$ and $^{1,3}E_b$ does not turn out to change the picture to a very significant extent. Indeed, a separate SCF calculation was performed on the weighted average of all ligand field states. The resulting orbitals were used in a full CI calculation within the same configuration space. The weight of the $b_2^2e^3a_1^1$ configuration in the final wavefunction of ^3E_a and ^1E_a was 0.91 and 0.86, respectively. In the ^3E_b and ^1E_b states on the other hand, the $b_2^2e^3b_1^1$ configurations were calculated with a weight of 0.89 and 0.82, respectively.)

In the five-coordinated complexes $Mn(CO)_5^+$ and $Mn(CO)_4Cl$ the relative ordering of both E states is self-evident, since in this case the axial axis is left with only one ligand. Yet, in $Mn(CO)_5Cl$ it is an indication of the fact that Cl^- should be classified as a weaker σ-donor than CO, in accordance with the classical ligand field picture. Due to the absence of an inversion centre in $Mn(CO)_5Cl$, both $^1A_1 \rightarrow {}^1E$ ligand field transitions are symmetry allowed. The two other spin allowed transitions, $^1A_1 \rightarrow {}^1A_2$ and $^1A_1 \rightarrow {}^1B_2$, however, are not. Therefore it is reasonable to assign both low-energy bands observed in the experimental absorption spectrum of $Mn(CO)_5Cl$ as ligand field $^1A_1 \rightarrow {}^1E$ transitions. This is further substantiated by the close correspondence between the experimental transition energies and the calculated results in Table 5: the first band, at 26 520 cm^{-1}, corresponds to the $^1A_1 \rightarrow {}^1E_a(xz,yz \rightarrow z^2)$ transition (calculated at 26 230 cm^{-1}); the second band, at 37 000 cm^{-1}, should be assigned as the $^1A_1 \rightarrow {}^1E_b(xz,yz \rightarrow x^2-y^2)$ transition (calculated at 35 642 cm^{-1}).

A comparison of the electronic absorption spectrum of $Mn(CO)_5Cl$ and the other halide complexes $Mn(CO)_5Br$ and $Mn(CO)_5I$ [25] shows that the relative position of analogous features in the three spectra can indeed be explained by qualitative ligand field arguments. The first band, situated at 26 520 cm^{-1} in $Mn(CO)_5Cl$, and assigned as $^1A_1 \rightarrow {}^1E(xz,yz \rightarrow z^2)$, shifts to a lower energy in $Mn(CO)_5Br$ (26 070 cm^{-1}), and even further in $Mn(CO)_5I$ (25 000 cm^{-1}). The relative position of this feature in the three spectra should be correlated with the spectrochemical strength of the corresponding halide ligand. This is indeed the case, as can be seen from the relative position of the halide ligands in the spectrochemical series [30]: I < Br < Cl. The position of the second band, assigned as $^1A_1 \rightarrow {}^1E(xz,yz \rightarrow x^2-y^2)$, is characterized by less significant shifts in the different spectra. Both in $Mn(CO)_5Cl$ and $Mn(CO)_5Br$ this feature shows up at 37 000 cm^{-1}, while in $Mn(CO)_5I$ a slightly lower energy is measured, namely 36 400 cm^{-1}. (In the experimental spectrum of $Mn(CO)_5I$ a third weak band appears at 33 600 cm^{-1}, between both $^1A_1 \rightarrow {}^1E$ transitions. We tentatively assign this band as the $^1A_1 \rightarrow {}^1A_2(xy \rightarrow x^2-y^2)$ ligand field transition in the equatorial plane (calculated at 32 657 cm^{-1} in $Mn(CO)_5Cl$). It is not clear why this feature only appears in the spectrum of $Mn(CO)_5I$, and not in the corresponding spectra of the other halide species.) The relative position of this band is related only to the π-donor properties of the halide ligand ($\Delta\pi$ in Table 5). The experimental band positions are thus indicative for an equal π-donor strength for Cl and Br, while I is a slightly stronger π-donor in the considered complexes.

It is also interesting to compare the ligand field spectrum of $Mn(CO)_5Cl$ with the analogous $HMn(CO)_5$ complex. The experimental spectrum of the latter complex is poorly resolved [27]. It shows only one ligand field band, appearing at a much higher energy than the first band in the spectrum of $Mn(CO)_5Cl$, namely at 34 500 cm^{-1}. Furthermore, in a recent *ab initio* study of the lowest excited states of $HMn(CO)_5$ this band has been identified as the $^1A_1 \rightarrow {}^1E$ transition corresponding to an ($xz,yz \rightarrow x^2-y^2$) excitation [31]. The second $^1A_1 \rightarrow {}^1E$ transition, corresponding to an ($xz,yz \rightarrow z^2$) excitation was calculated about 10 000 cm^{-1} higher in energy. This result indicates that in $HMn(CO)_5$ the axial σ-donation is stronger than the σ-donation in the equatorial plane. Therefore, as opposed to Cl^-, H^- should be classified as a stronger σ-donor than CO. The reversed order of the $^1A_1 \rightarrow {}^1E$ transitions in both complexes is bound to have important consequences on their photochemical behaviour. Thus in $Mn(CO)_5Cl$ the first ligand field excitation, corresponding to a z^2 population, can be expected to result in a weakening of the axial CO bond. In $HMn(CO)_5$ on the other hand the first $^1A_1 \rightarrow {}^1E$ transition results in an x^2-y^2 population, and should therefore be the precursor of an equatorial CO loss. In a subsequent paper [17] we will discuss the photochemical behaviour of $Mn(CO)_5Cl$. An *ab initio* study of the photochemistry of $HMn(CO)_5$, including Contracted Configuration Interaction calculations based on Complete Active Space SCF wavefunctions, has been reported very recently [32]. However this study does not consider the possibility of an equatorial CO dissociation in this complex.

A very striking feature of Fig. 1 is the extremely strong stabilization in the five-coordinated complexes

$Mn(CO)_5^+$ and $Mn(CO)_4Cl$ of both the B_2 and E_a states (singlet and triplet), which are characterized by a partial occupation of the $a_1(\sim 3d_{z^2})$ orbital. In $Mn(CO)_4Cl$, this stabilization is found to be so extreme as to result (at the Hartree–Fock level of sophistication) in a ^3E_a ground state. According to the Hartree–Fock calculations, this state is calculated at 514 cm^{-1} below the $^1A_1$ state. However, since electron correlation will almost certainly lower the energy of $^1A_1$ to a much larger extent than ^3E, the experimental ground state is quite likely to remain a $^1A_1$ state. Both states can however be expected to lie very close to each other even after the inclusion of correlation effects. This is substantiated by the above mentioned *ab initio* study of the photochemistry of $HMn(CO)_5$ [32]. In the square pyramid $HMn(CO)_4$, resulting from the loss of an axial carbonyl ligand from $HMn(CO)_5$, the lowest ^3E state is also calculated less than 2000 cm^{-1} apart from the $^1A_1$ ground state. The close proximity of both states makes intersystem crossing between them an easy process, and can thus play an important role in the photochemistry of monosubstituted d^6 carbonyl species.

It is clear that the energetic evolution of the states under consideration can by no means be rationalized by the first-order ligand field expressions of Table 5. Thus one would have to invoke a value of $\sigma_{CO} = 25\,900$ cm^{-1} and of $\sigma_{Cl} = 19\,300$ cm^{-1} in order to be able to account for the large stabilization of the $^1B_2$ state caused by the dissociation of CO from $Mn(CO)_6^+$ or the dissociation of Cl^- from $Mn(CO)_5Cl$, both resulting in $Mn(CO)_5^+$. Similar extreme values are obtained by considering the evolution of the other states under consideration.

In the next section we will show that the unusually low energy of the relevant states is caused by mixing of metal 4s and $4p_z$ orbitals into the a_1 $(\sim 3d_{z^2})$ orbital.

C. d-s-p mixing as a rationale for the low lying B_2 and E states

Though ligand field theory is essentially a d-only model, occasionally it was realized that under certain symmetry conditions, the 4s, and also the 4p orbitals [33–35] could mix with the 3d orbitals, thereby altering their bonding characteristics. On many occasions however, this mixing can be considered to be only of secondary importance [36]. Previously [5, 6], it was shown that a d-only ligand field picture is indeed quite capable of rationalizing the Hartree–Fock results for the ligand field spectrum of mono- and disubstituted Co(III) cyanide complexes.

However, due to the low formal charge of the central metal ion, d–s and even d–p transitions do occur at a rather low energy in the hexacarbonyl complexes of V^-, Cr and Mn^+, but in these octahedral compounds, orbital mixing of the 3d-type orbitals with either 4s or 4p is symmetry forbidden. As can be seen from Table 1, the reduction in symmetry from O_h to C_{4v} induces the mixing of 4s and 4p into the 3d-type orbitals both within the $a_1(d_{z^2}$, s and $p_z)$ and the e representations (d_{xz}, d_{yz} with p_x, p_y), respectively.

This is further illustrated in Table 6, showing the different 3d-type orbitals in the $^3E_a(xz,yz \rightarrow z^2)$ state, as well as their composition in terms of the metal atomic orbitals. While d–p mixing is very limited within the π-type e shell, d–s as well as d–p mixing turn out to be rather important within the σ bonding $a_1(\sim 3d_{z^2})$ orbital, especially in the five-coordinated complexes $Mn(CO)_4Cl$ and $Mn(CO)_5^+$. In the latter we find a total s–p contribution of 15%, which is even larger than the contribution of the ligand orbitals.

In a perturbational context, it may be useful to introduce the intermediate orbital $a_1'(\sim 3d_{z^2})$ which is a linear combination of ligand orbitals and metal $3d_{z^2}$ orbitals only. The low symmetry components of the ligand field are able to mix $a_1'(\sim 3d_{z^2})$ with components of the higher lying vacant 4s and 4p orbitals, so as to yield the final $a_1(\sim 3d_{z^2})$ orbital. This mixing will always result in an extra stabilization of the hypothetical $a_1'(\sim 3d_{z^2})$ orbital, due to the altered bonding capabilities of the metal $d^x s^y p^z$ hybrids. This extra stabilization is at the basis of the low energy of the relevant C_{4v} states in Fig. 1 ($^3B_2$, $^1B_2$, ^3E_a and ^1E_a) as compared to the octahedral $Mn(CO)_6^+$.

The sign and magnitude of the mixing of the 4s and 4p orbitals will be such as to weaken the bonding along certain spatial directions and to enhance the bonding in other directions. More specifically, since the $a_1'(\sim 3d_z)$ orbital is a metal–ligand antibonding orbital, mixing will occur with a phase relationship allowing this antibonding to decrease. In this respect it is instructive to consider the d–s and d–p mixing separately:

(i) d–s mixing results in a decrease of the overlap of the $a_1'(\sim 3d_{z^2})$ orbital with the four strong CO ligands in the equatorial plane. This decrease can only take place if at the same time the overlap with the axial ligands is increased. This is illustrated in Fig. 2 for the $^3E(xz,yz \rightarrow z^2)$ state in $Mn(CO)_4Cl$. In this Figure the metal part of the $17a_1$ orbital is decomposed into its different atomic orbital components. While Fig. 2(a) only shows the $3d_{z^2}$ part, in Fig. 2(b) the 4s part is added. One can clearly see how d–s mixing results in a contraction of the equatorial lobe of the d_{z^2} orbital, whereas the axial

TABLE 6. Orbital energy (in Ha) and procentual composition of the 3d-type orbitals in the ^3E_a states of the C_{4v} complexes $Mn(CO)_5^+$, $Mn(CO)_5Cl$ and $Mn(CO)_4Cl$

	Symmetry C_{4v}	Energy	Mn			CO_{eq}			CO_{ax}		Cl	
			3d	4s	4p	σ	$\pi_\parallel$	$\pi_\perp$	σ	π	s,p$_\sigma$	p$_\pi$
$Mn(CO)_5^+$	$17a_1$	−0.6149	76	3	12	3		4	3			
	$2b_2$	−0.6310	84				16					
	11e	−0.6567	94					4		2		
$Mn(CO)_5Cl$	$2b_2$	−0.4427	83				17					
	$22a_1$	−0.4453	87	1	1	4			4		3	
	12e	−0.4498	90		1			4		3		2
$Mn(CO)_4Cl$	$2b_2$	−0.4213	82				18					
	$17a_1$	−0.4563	84	4	6	2		3			1	
	11e	−0.4723	95					3				2

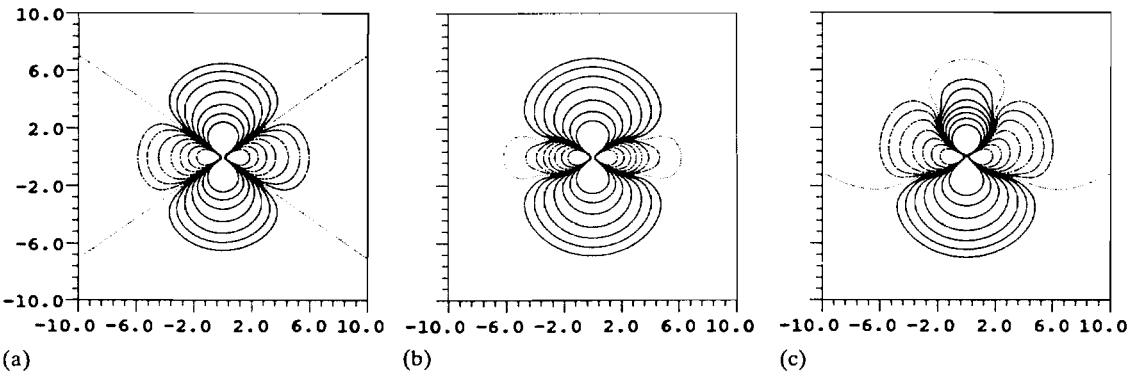

Fig. 2. Metal atomic orbital contributions to the $17a_1(\sim 3d_{z^2})$ orbital in the ^3E_a ground state of $Mn(CO)_4Cl$. (a) $3d_{z^2}$, (b) $3d_{z^2}+4s$, (c) $3d_{z^2}+4p$. The figures are drawn in the xz plane. The interatomic distances are given in a.u. Full contours correspond to positive values and dashed contours to negative values of ψ, while dotted lines represent nodal planes. The values of the ψ contours are ± 0.00125, ± 0.0025, ± 0.005, ± 0.01, ± 0.02, ± 0.04 and ± 0.08 a.u.$^{-3/2}$.

lobe is expanded. The corresponding strengthening of the equatorial bonds and the concomitant weakening of the axial bonds do cancel exactly in the octahedral case. But if one axial ligand is removed (as in $Mn(CO)_4Cl$ or in $Mn(CO)_5^+$), the system is obviously stabilized by 3d–4s mixing, with the phase combination shown in Fig. 2. The mixing will become more favourable as the difference in the mean overlap of the equatorial and axial ligands increases, or in the following order

$$\text{3d–4s: } Mn(CO)_4Cl > Mn(CO)_5^+ > Mn(CO)_5Cl \quad (6)$$

which is confirmed by the population analysis results in Table 6.

(ii) d–p mixing will not significantly affect the σ bonding with the equatorial CO ligands, which are situated in the nodal plane of the $4p_z$ orbital. But it certainly will be important for axial bonding since it is able to reinforce one lobe of $3d_{z^2}$ at the expense of the other lobe. d–p mixing can thus be expected to become more important as the difference in σ strength of both axial sites increases. This is especially important in the five-coordinated complexes, where one of the axial sites is vacant. The $a_1'(\sim 3d_{z^2})$ orbital can then be reshaped by hybridization with $4p_z$, so as to reduce the electron density in the direction of the remaining axial ligand, while at the same time increasing its spatial extension toward the missing ligand site. This is illustrated in Fig. 2(c), showing the sum of the $3d_{z^2}$ and the $4p_z$ part of the $17a_1$ orbital in the $^3E_a(d_{xz,yz} \rightarrow d_{z^2})$ state of $Mn(CO)_4Cl$. The effect is even more pronounced in $Mn(CO)_5^+$, due to the very large σ strength of the remaining axial CO ligand in this complex. This can be seen in Fig. 3, where the relevant a_1 orbitals are shown for the three complexes $Mn(CO)_5Cl$, $Mn(CO)_5^+$ and $Mn(CO)_4Cl$, together with their total metal contribution. The d–p mixing clearly decreases in the order

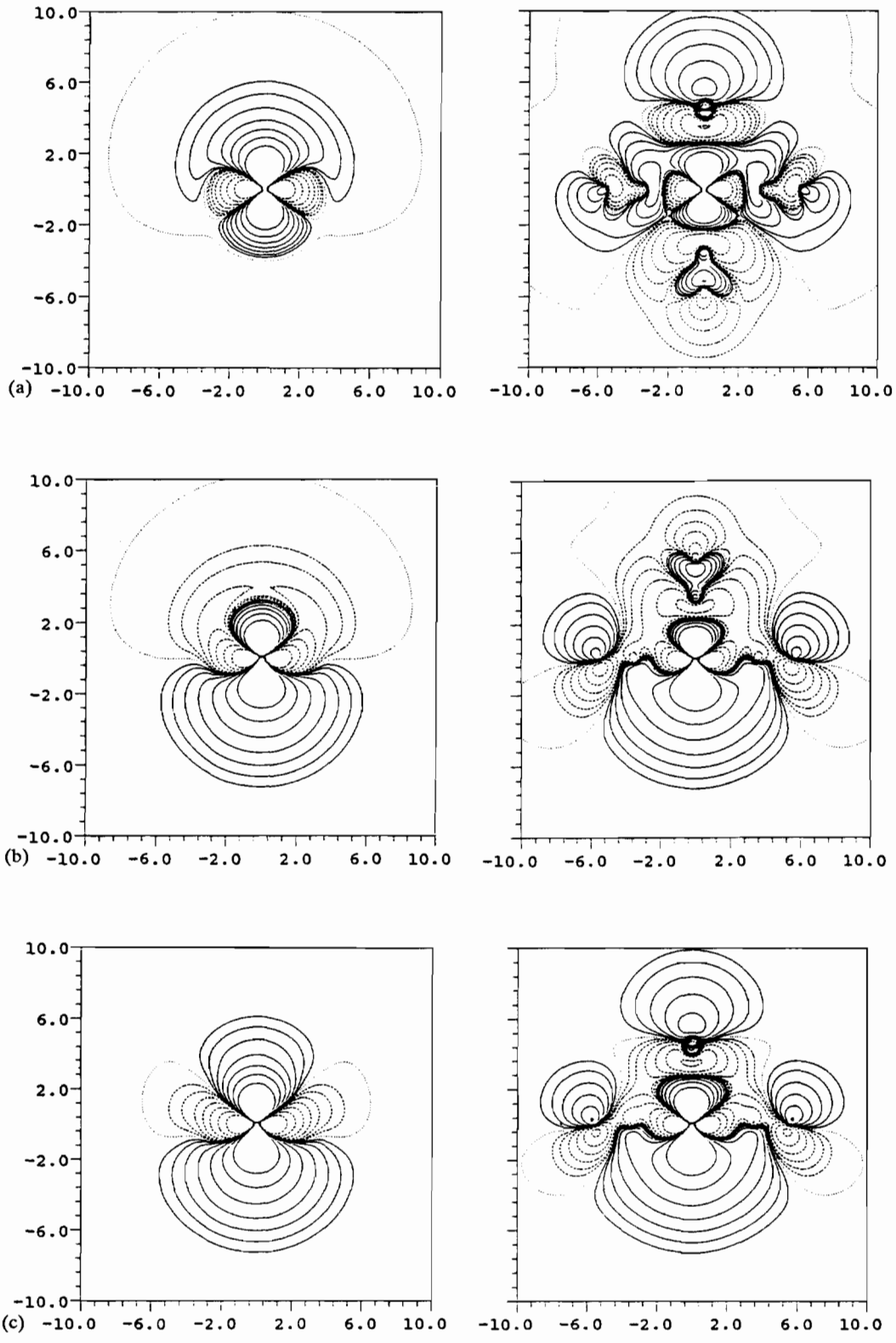

Fig. 3. The $a_1(\sim 3d_{z^2})$ σ antibonding orbital (right) and its total metal atomic contribution (left), for the $^3E_a(xz,yz \rightarrow z^2)$ state. (a) $Mn(CO)_5Cl$, (b) $Mn(CO_5)^+$, (c) $Mn(CO)_4Cl$. All figures are drawn in the xz plane. The interatomic distances are given in a.u. Full contours correspond to positive values and dashed contours to negative values of ψ, while dotted lines represent nodal planes. The values of the ψ contours are ± 0.00125, ± 0.0025, ± 0.005, ± 0.01, ± 0.02, ± 0.04 and ± 0.08 a.u.$^{-3/2}$.

$$3d\text{–}4p: Mn(CO)_5^+ > Mn(CO)_4Cl > Mn(CO)_5Cl \quad (7)$$

which is again confirmed by the results in Table 6. It is also interesting to note (Fig. 3(a) versus (c)) how the 3d–4p_z mixing takes place with a *different sign* in $Mn(CO)_4Cl$ and $Mn(CO)_5Cl$, thereby in each case expanding the electron density in the direction of the weakest axial σ donor.

Conclusions

From the results of a Mulliken population analysis on the ground state of the four considered carbonyl complexes one may conclude that the classical concept of ligand additivity, originally formulated for an ionic bonding model, is consolidated (at least at the Hartree–Fock level) for the more covalent metal–carbonyl complexes.

Some of the broad features of the calculated ligand field spectra can also be reproduced quite satisfactorily with a ligand field parametrization scheme. The equatorial ligand field strength is seen to be independent of the presence of axial ligands. Cl^- is characterized as a π-donor, while a negative π-parameter should indeed be assigned to CO. Based on our calculations, the weak features in the experimental UV–Vis spectrum of $Mn(CO)_5Cl$ are assigned at the $^1A_1 \rightarrow {}^1E$ symmetry allowed ligand field transitions. The relative position of the two ^1E states, $^1E_a(xz,yz \rightarrow z^2)$ and $^1E_b(xz,yz \rightarrow x^2\text{–}y^2)$, is connected with the difference in σ-donor strength between CO and Cl^-: $\sigma_{Cl} < \sigma_{CO}$.

Finally it is shown that 3d–4s–4p mixing in the σ-antibonding $a_1(\sim 3d_{z^2})$ orbital causes a substantial stabilization of some of the excited triplet states ($^3B_2$ and ^3E_a) in the five-coordinate square pyramids.

Acknowledgement

We are indebted to the Belgian Government (Programmatie van het Wetenschapsbeleid) for financial support.

References

1 F. A. Cotton and G. Wilkinson, *Advanced Inorganic Chemistry,* Wiley, New York, 5th edn., 1988.
2 M. Gerloch, *Coord. Chem. Rev., 99* (1990) 117.
3 L. G. Vanquickenborne, L. Haspeslagh, M. Hendrickx and J. Verhulst, *J. Inorg. Chem., 23* (1984) 1677.
4 L. G. Vanquickenborne, M. Hendrickx, D. Postelmans, I. Hyla-Kryspin and K. Pierloot, *Inorg. Chem. 27* (1988) 900.
5 L. G. Vanquickenborne, M. Hendrickx, I. Hyla-Kryspin and L. Haspeslagh, *Inorg. Chem., 25* (1986) 885.
6 L. G. Vanquickenborne, M. Hendrickx and I. Hyla-Kryspin, *Inorg. Chem., 28* (1989) 770.
7 L. G. Vanquickenborne, K. Pierloot and D. Devoghel, *Inorg. Chem., 28* (1989) 1805.
8 L. G. Vanquickenborne and A. Ceulemans, *J. Am. Chem. Soc., 99* (1977) 2208.
9 C. C. J. Roothaan, *Rev. Mod. Phys., 32* (1960) 179.
10 G. A. Van der Velde, *Ph.D. Thesis,* Rijksuniversiteit Groningen, The Netherlands, 1974.
11 S. J. La Placa, W. C. Hamilton, J. A. Ibers and A. Davidson, *Inorg. Chem., 8* (1969) 1928.
12 R. F. Bryan, P. T. Green and A. R. Manning, *Abstr. American Crystallographic Association, Seattle, WA, Mar. 1969,* M6.
13 P. T. Greene and R. F. Bryan, *J. Chem. Soc. A, 10* (1971) 1559.
14 M. F. Guest, M. B. Hall and I. H. Hillier, *Mol. Phys., 25* (1973) 629.
15 (a) R. N. Perutz and J. J. Turner, *Inorg. Chem., 14* (1975) 266; (b) S. P. Church, M. Poliakoff, J. A. Timmey and J. J. Turner, *J. Am. Chem. Soc., 103* (1981) 7515; (c) T. M. McHugh, A. J. Rest and D. J. Taylor, *J. Chem. Soc., Dalton Trans.,* (1980) 1803.
16 R. D. Davy and M. B. Hall, *Inorg. Chem., 28* (1989) 3524.
17 K. Pierloot, P. Hoet and L. G. Vanquickenborne, to be published.
18 T. H. Dunning, *J. Chem. Phys., 53* (1970) 2823; S. Huzinaga, *J. Chem. Phys., 42* (1965) 1293.
19 T. H. Dunning, *Chem. Phys. Lett., 7* (1970) 423.
20 L. G. Vanquickenborne and J. Verhulst, *J. Am. Chem. Soc., 105* (1983) 1769.
21 J. Demuynck, A. Veillard and U. Wahlgren, *J. Am. Chem. Soc., 95* (1973) 5563.
22 M. Sano, Y. Hatano, H. Kashiwagi and H. Yamatera, *Bull. Chem. Soc. Jpn., 54* (1981) 1523.
23 D. L. Lichtenberger, A. C. Sarapu and R. F. Fenske, *Inorg. Chem., 12* (1973) 702.
24 R. F. Fenske and R. L. De Kock, *Inorg. Chem., 9* (1970) 1053.
25 L. G. Vanquickenborne and A. Ceulemans, *Coord. Chem. Rev., 48* (1983) 157.
26 N. A. Beach and H. B. Gray, *J. Am. Chem. Soc., 90* (1968) 5713.
27 G. B. Blakney and W. F. Allen, *Inorg. Chem., 10* (1971) 2763.
28 K. Pierloot, J. Verhulst, P. Verbeke and L. G. Vanquickenborne, *Inorg. Chem., 28* (1989) 3059.
29 G. L. Geoffroy and M. S. Wrighton, *Organometallic Photochemistry,* Academic Press, New York, 1979.
30 M. Gerloch and R. C. Slade, *Ligand-field Parameters,* Cambridge University Press, Cambridge, 1973.
31 A. Veillard, A. Strich, C. Daniel and P. E. M. Siegbahn, *Chem. Phys. Lett., 141* (1987) 329.
32 C. Daniel, *Coord. Chem. Rev., 97* (1990) 141.
33 A. Ceulemans, D. Beyens and L. G. Vanquickenborne, *Inorg. Chim. Acta, 61* (1982) 199.
34 M. Elian and R. Hoffmann, *Inorg. Chem., 14* (1975) 1058.
35 M. Elian and R. Hoffmann, *Inorg. Chem., 15* (1976) 212.
36 J. K. Burdett, *Inorg. Chem., 14* (1975) 931.

Appendix

Starting from a set of three normalized contracted Gauss type functions (CGTF) χ_1, χ_2 and χ_3, the following non-segmented basis functions can be constructed:

$$\varphi_1 = a\chi_1 + b\chi_2$$
$$\varphi_2 = r\chi_2 + s\chi_3 \quad (1')$$

This operation will lead to a minimal energy loss if, for any occupied orbital i, the following equation holds:

$$d_{1i}\chi_1 + d_{2i}\chi_2 + d_{3i}\chi_3 = c_{1i}\varphi_1 + c_{2i}\varphi_2 \quad (2')$$

In this equation d_{1i}, d_{2i} and d_{3i} represent the coefficients of the original CGTF in orbital i, while c_{1i} and c_{2i} stand for the final, unknown coefficients. By combining the eqns. (1') and (2') the following set of equations can be deduced:

$$d_{2i} = \frac{b}{a} d_{1i} + \frac{r}{s} d_{3i} \quad (3')$$

with i running over all occupied orbitals.

The ratios $\frac{a}{b}$ and $\frac{r}{s}$ can now easily be obtained by a least-squares fitting procedure. The following Table shows the exponents and contraction coefficients of the (15s 11p 6d/9s 6p 4d) non-segmented basis set for the Mn atom, that were obtained by the above procedure.

Exponents	Coefficients	Exponents	Coefficients
s-set		p-set	
243694	0.005191	1500.39	−0.002372
35995	0.040272	358.8	−0.018830
8223.56	0.206195	116.699	−0.085445
2353.12	0.816003	44.6132	−0.785262
780.965	2.017909	18.5985	−1.291673
288.519	4.523658	44.6132	−1.820281
780.965	0.045878	18.5985	−2.994171
288.519	0.102847	8.13778	1.000000
115.701	0.679651	3.33734	1.000000
49.1175	0.349546	1.37895	−0.113948
16.0885	1.000000	1.37895	2.263438
6.7043	1.000000	0.538639	1.000000
1.80517	1.000000	0.229000	1.000000
0.703011	1.000000	0.094000	1.000000
0.264000	1.000000		
0.095000	1.000000		
0.034000	1.000000		

d-set	
42.63	0.016715
11.97	0.094015
4.091	0.260780
1.45	1.000000
0.47	1.000000
0.1281	1.000000